The Martensitic Transformation in Cobalt

R. T. Johnson Jr. and R. D. Dragsdorf

Citation: Journal of Applied Physics **38**, 618 (1967); doi: 10.1063/1.1709384
View online: http://dx.doi.org/10.1063/1.1709384
View Table of Contents: http://scitation.aip.org/content/aip/journal/jap/38/2?ver=pdfcov
Published by the AIP Publishing

are free to rotate at X-band frequencies (up to the critical hydration). It is also of interest to note that the measurement of the Faraday rotation vs the magnetic field shows linear dependence. This result is further proof of the validity of Eq. (22).

As the amount of adsorbed water increases beyond the critical hydration, the free water molecules (monomers which are bound by hydrogen bonds to the polar groups of hemoglobin, such as $-NH_2$ and $-COOH$) start to form hydrogen-bonded clusters (dimers, trimers, etc.) and result in an icelike structure on the surface of the hemoglobin. Since the frequency dependence of the dielectric constant of ice shows that water molecule dipoles in ice structure undergo relaxation at frequencies somewhere near 10 kc/sec,[4] the water molecules bound into an icelike structure on the hemoglobin are unable to orient as the free water molecules at microwave frequencies. In this case, bound water appears irrotational at high microwave frequencies.

A qualitative theory about the effect of water on a hemoglobin surface is still lacking, but it is believed that this experiment confirms the theory which is based on the dipole relaxation of the bound water.

ACKNOWLEDGMENTS

The authors wish to thank Dr. M. Orentlicher at Columbia University for his helpful discussions. Thanks are also due to F. Clapp, R. Cruse, and W. Zeilinger for their technical assistance, and to Miss K. Howard for her assistance in preparing hemoglobin samples.

JOURNAL OF APPLIED PHYSICS VOLUME 38, NUMBER 2 FEBRUARY 1967

The Martensitic Transformation in Cobalt*

R. T. Johnson, Jr.,† and R. D. Dragsdorf
Department of Physics, Kansas State University, Manhattan, Kansas

(Received 2 September 1966)

The properties of the fcc to hcp transformation in cobalt single-crystal whiskers have been determined. Studies of the crystallographic properties and dislocation structure using optical, standard x-ray diffraction, and high-resolution x-ray diffraction topographic techniques are herein reported. It is shown that the atomic movements associated with the transformation in cobalt initiate at the most highly strained regions in the crystal. The strain configuration and the crystal boundaries act as a combined mechanism restricting the transformation to a particular set of {111} planes. When the strain distribution is nonuniform throughout the crystal, localized regions within the crystal utilize different sets of {111} transformation planes. The transformation from the fcc to hcp phase is accomplished by the glide of Shockley partial dislocations through the lattice. Frank partial dislocations remain pinned in the lattice. These partials are formed from the extension of total dislocations. Martensitic platelets result from either the glide of Shockley partial dislocations which have different slip vectors in parallel and adjacent sections of the crystal or the pinning of Frank partial dislocations which form the boundary of faulted regions. The platelets intersecting the crystal surfaces produce observable slip bands.

INTRODUCTION

THE role of dislocations in the martensitic face-centered cubic, fcc, to the hexagonal close-packed, hcp, transformation in cobalt[1–4] has been in doubt. This has been partially due to the difficulty of identifying the orientation and types of dislocations that have been formed as a result of the transformation. New x-ray diffraction techniques[5–8] have eliminated this obstacle. Individual dislocations can now be resolved and identified.[9]

Several researchers[10–13] have realized that dislocations are probably tied to the glide movements prop-

* This work was supported by the Bureau of General Research at Kansas State University and was submitted as partial fulfillment of the requirements for the Ph.D. degree.

† Present address: Sandia Corporation, Albuquerque, New Mexico.

[1] A. R. Troiano and J. L. Tokich, Trans. AIME **175**, 728 (1948).

[2] J. S. Bowles and J. K. Mackenzie, Acta Met. **2**, 129–147 (1954); B. A. Bilby and J. W. Christian, *The Mechanism of Phase Transformations in Metals* (Institute of Metals, London, 1956), pp. 121–172.

[3] F. Sebilleau and H. Bibring, *The Mechanism of Phase Transformations in Metals* (Institute of Metals, London, 1956), pp. 209–217.

[4] P. Gaunt and J. W. Christian, Acta Met. **7**, 529 (1959).

[5] W. W. Webb, in *Direct Observations of Imperfections in Crystals*, J. B. Newkirk and J. H. Wernick, Eds. (Interscience Publishers, New York, 1962), p. 26; J. Appl. Phys. **31**, 194 (1960).

[6] A. R. Lang, J. Appl. Phys. **30**, 1748 (1959); **29**, 597 (1958); Acta Met. **5**, 358 (1957); Acta Cryst. **12**, 249 (1959).

[7] J. B. Newkirk, J. Metals **14**, 661 (1962); Trans. AIME **215**, 483 (1959); Phys. Rev. **110**, 1465 (1958); J. Appl. Phys. **29**, 995 (1958).

[8] S. Amelinckx, *The Direct Observation of Dislocations* (Academic Press, New York, 1964), Solid State Physics, Supplement 6, p. 90.

[9] U. Bonse, Z. Physik **153**, 278 (1958); in *Direct Observations of Imperfections in Crystals*, J. B. Newkirk and J. H. Wernick, Eds. (Interscience Publishers, New York, 1962), p. 431.

[10] A. Seeger, Z. Metallk. **44**, 247 (1953); **47**, 653 (1956).

[11] J. W. Christian, Proc. Roy. Soc. (London) **206A**, 51 (1951).

[12] B. A. Bilby, Phil. Mag. **44**, 782 (1953).

[13] Z. S. Basinski and J. W. Christian, Phil. Mag. **44**, 791 (1953).

agating the martensitic transformation. Votava[14] using electron microscopy has shown that the transformation in thin films does proceed with the aid of partial dislocations. Dehlinger *et al.*[15] suggested that the transformation occurs preferentially on those cubic {111} planes which have the greatest surface area, and Stadelmaier and Hook[16] argued that initiation does not occur until an energy barrier of the magnitude of the surface or interfacial energy is overcome. It is reasonable to expect that the transformation process is also strongly influenced by the lattice strain of the imperfection structure.

The fcc and hcp phases of cobalt are in thermal equilibrium at 417°C.[17] The transformation from the high-temperature fcc phase to the hcp phase is most often incomplete.[18,19] Both growth and deformation faults have been identified in the hcp phase.[20,21] Large faulted regions produced by macroscopic shear result in the formation of thin martensitic platelets.[22–25] These platelets lie parallel to the transformation plane and produce slip bands when they intersect the crystal boundaries. The formation of these platelets may be related to a dislocation mechanism since Frank and Shockley partial dislocations form the boundaries where stacking faults terminate inside close-packed crystals.[26]

The purpose of this paper is to relate the dislocation structure and the crystallographic properties of cobalt whiskers to the transformation. Cobalt single-crystal whiskers were examined because of their high-purity, low-dislocation population, and easily defined crystallographic axes. Detailed relationships between the whisker axes, the crystal boundaries, the slip band formations, and the dislocation structure were obtained using optical, standard x-ray diffraction, and high-resolution x-ray diffraction topographic techniques.

CRYSTALLOGRAPHY

The transformation from the fcc lattice to the hcp lattice can be accomplished by a series of glide movements parallel to any of the four sets of {111} planes in the fcc structure. The reverse hcp to fcc transformation can occur similarly on only the (00·1) plane of the hcp system. The atomic displacements result in a homogeneous deformation which is expressed mathematically as linear functions of the coordinates.

Consider the transformation from the fcc to the hcp structure which takes place on the (111) set of cubic planes. The resulting hcp unit cell vectors, $\mathbf{a}_i$, are related to the initial fcc unit cell vectors, $\mathbf{A}_i$, by the matrix equation: $\mathbf{a}=B\mathbf{A}$, where

$$B=\frac{1}{6}\begin{bmatrix}-3 & 3 & 0\\ 0 & -3 & 3\\ 4 & 4 & 4\end{bmatrix}.$$

If the transformation occurs on any one of the other three sets of {111} planes, a similar transformation matrix is obtained.

The displacement resulting in the transformation is most likely to occur in one of three directions on the slip plane. The possible slip vectors for transformation in the (111) plane are $[11\bar{2}]$, $[1\bar{2}1]$, and $[\bar{2}11]$. Equivalent directions in the fcc and hcp structures can also be specified. An arbitrary vector $\boldsymbol{\rho}$ can be expressed in terms of either $\boldsymbol{\rho}=\sum_i Q_i\mathbf{A}_i$ or $\boldsymbol{\rho}=\sum_i q_i\mathbf{a}_i$, where $i=1, 2, 3$. The coordinates of a point in the fcc and hcp systems are denoted by Q_i and q_i, respectively. $Q=\tilde{B}q$ represents the transformation as having occurred on the (111) set of planes. $\tilde{B}$ is the transpose of B.

Corresponding planes in the fcc and hcp systems have the same reciprocal lattice vector, $\mathbf{G}$. This vector can be expressed in terms of either the Miller indices HKL for the fcc system or hkl for the hcp system. The B matrix relates hkl and HKL. The planes parallel to the axis of a whisker have been determined by setting $\boldsymbol{\rho}_0\cdot\mathbf{G}=0$, where $\boldsymbol{\rho}_0$ is here a vector representing the whisker axis.

EXPERIMENTAL

Cobalt whiskers were grown in the high-temperature phase by hydrogen reduction of $CoCl_2$ but were cooled through the phase transformation to the hcp structure before being examined at room temperature. The growth procedure and general properties of the whiskers have already been reported.[27] Sixty single-crystal whiskers were analyzed in this study.

The axis and crystallographic phase of the whiskers were determined from x-ray rotation patterns. The planes which formed the crystal boundaries were identified by utilizing a Nonius optical goniometer in conjunction with x-ray diffraction techniques. Slip band formations on the surfaces of the whiskers were examined with a Leitz ortholux microscope with ultrapak objectives having an upper numerical aperture of 0.65.

[14] E. Votava, J. Inst. Metals **90**, 129 (1961).
[15] V. U. Dehlinger, E. Osswald, and H. Bumm, Z. Metallk. **25**, 62 (1933).
[16] H. H. Stadelmaier and R. C. Hook, Acta Met. **4**, 223 (1956).
[17] J. B. Hess and C. S. Barrett, J. Met. **4**, 645 (1952).
[18] O. S. Edwards and H. Lipson, Proc. Roy. Soc. (London) **180A**, 268 (1942); J. Inst. Metals **69**, 177 (1943).
[19] E. A. Owen and D. M. Jones, Proc. Phys. Soc. (London) **67B**, 456 (1954).
[20] T. R. Anantharaman and J. W. Christian, Acta Cryst. **9**, 479 (1956).
[21] C. R. Houska, B. L. Averbach, and M. Cohen, Acta Met. **8**, 81 (1960).
[22] T. R. Anantharaman and J. W. Christian, Phil. Mag. **43**, 1338 (1952).
[23] V. J. Kehrer and H. Leidheiser, Jr., J. Chem. Phys. **21**, 570 (1953).
[24] H. Bibring and F. Sebilleau, Compt. Rend. **239**, 54 (1954).
[25] M. J. Bibby and J. G. Parr, Cobalt **20**, 111 (1963).
[26] W. T. Read, *Dislocations in Crystals* (McGraw-Hill Book Company, Inc., New York, 1953), p. 93.
[27] R. D. Dragsdorf and R. T. Johnson, Jr., J. Appl. Phys. **33**, 724 (1962).

Screw dislocations which had components parallel to the whisker axis were identified using an x-ray diffraction technique developed by Dragsdorf and Webb.[28] Continuous radiation was diffracted from planes parallel to the whisker axis and was recorded on a cylindrical camera coaxial with the whisker. The lattice twist which results from the screw dislocation[29] was determined from the tilt of the equatorial Laue spots. The component of the Burgers vector parallel to the whisker axis was determined from the product of the lattice twist, whisker cross-sectional area, and a geometric constant. The lattice twist and dislocation Burgers vector were also determined from the resolved separation of the $K\alpha_1$ and $K\alpha_2$ maxima when characteristic radiation was used. The magnitude of the Burgers vector $\mathbf{b}$ was determined from the expression $|b| = C\Delta\theta/Ks$, where $\Delta\theta$ is the angular separation of the $K\alpha_1$ and $K\alpha_2$ diffraction beams, s is the distance between the centers of the $K\alpha_1$ and $K\alpha_2$ diffraction images, C is the whisker cross-sectional area, and K is a geometric constant.

The density, magnitude, and orientation of other dislocations were determined by using a high-resolution x-ray diffraction topography technique similar to the Berg–Barrett method.[30] Dislocations were detected and mapped by recording local perturbations in the diffracting power in the vicinity of the dislocations.

A microfocus x-ray unit with a cobalt target was used to provide a high specific intensity of x rays. The tube was operated at 34 kV which gave a focal spot diameter of 30 μ and beam divergence at the whisker of 6 sec of arc. The crystal was oriented to diffract the characteristic $K\alpha$ radiation from a specific set of crystallographic planes. The diffracted beam was recorded on nuclear track plates (Eastman NTB and Ilford K.5) with emulsion thicknesses of 10 μ. The emulsion was positioned from 1 to 3 mm from the crystal and was oriented so that the diffracted beam was perpendicular to the plate. Exposure times were several minutes. Numerous topographs were normally taken about a diffraction peak by slightly changing the orientation of the crystal between exposures. Some high-resolution photographs were also taken while the whisker was oscillating (± 0.25, ± 0.35, or $\pm 0.75°$) about a diffraction maxima.

A theory for the diffraction contrast from dislocations has been proposed by Bonse.[9] He showed that the change in intensity caused by a dislocation is proportional to $(M/r)\mathbf{b}\cdot\mathbf{G}$, where r is the radial distance from the dislocation line and M is the slope of the experimental rocking curve. His theory predicts that the maximum intensity contrasts occur when the dislocation Burgers vector is perpendicular to the diffraction planes. No contrast occurs when $\mathbf{b}\cdot\mathbf{G}=0$. The contrast may appear as a region of light or dark contrast with respect to the background depending upon the orientation of the crystal with respect to the diffraction maximum. For this experiment a 20% intensity change was assumed to be detectable. The minimum detectable lattice orientation change corresponding to these assumptions is about 8 sec of arc. The maximum distance from a dislocation at which intensity contrasts are detectable is 1.5 μ for a Burgers vector of 4 Å. These results, in conjunction with other resolution considerations (diffraction geometry, experimental apparatus, and emulsion), showed that dislocations separated by 3 μ should be resolved when using this x-ray diffraction topographic technique.

OBSERVATIONS

The majority of the whiskers examined were from 1 to 20 μ in cross-sectional dimension and were several millimeters in length. The transformation from the as-grown fcc phase to the hcp phase was never complete. From 5% to 10% of the cubic phase was retained at room temperature.

Axes

The whiskers had axes in the $\langle 10\cdot 0\rangle$, $\langle 11\cdot 1\rangle$, $\langle 12\cdot 2\rangle$, $\langle \bar{1}1\cdot 1\rangle$, and $\langle 00\cdot 1\rangle$ directions in the hcp system. The relationships between these axes and the axes of the initial, as-grown, fcc whiskers are summarized in Table I. The majority of the cobalt whiskers grew with axes corresponding to the direction of closest packing in the fcc phase, i.e., the $\langle 110\rangle$ direction.[27] The hcp $\langle 10\cdot 0\rangle$, $\langle 11\cdot 1\rangle$, and $\langle 12\cdot 2\rangle$ axes resulted from initial $\langle 110\rangle$ fcc whiskers. The $\langle 11\cdot 1\rangle$ and $\langle 12\cdot 2\rangle$ axes resulted from transformation on the same set of $\{111\}$ planes while the $\langle 10\cdot 0\rangle$ whiskers had a different set of slip planes. Only four of the sixty whiskers were found to grow with initial $\langle 100\rangle$ fcc axes. Slip occurring on any of the four sets of $\{111\}$ planes of this whisker resulted in the observed $\langle \bar{1}1\cdot 1\rangle$ set of hcp axes. The hcp $\langle 00\cdot 1\rangle$ and $\langle \bar{2}2\cdot 1\rangle$ axes both could have resulted from an initial $\langle 111\rangle$ fcc whisker, but only the $\langle 00\cdot 1\rangle$ whiskers were observed.

Some of the whiskers were slightly kinked. The kinking was caused by a shift in the whisker axis that resulted from the transformation. The analysis summarized in Table I shows that an exact correlation between the initial fcc and observed hcp axes occurs only for the whiskers with $\langle 10\cdot 0\rangle$ and $\langle 00\cdot 1\rangle$ axes. Thus, the axes of these whiskers remained fixed during the transformation. These whiskers were observed to be generally straight and uniform. Whiskers with $\langle 11\cdot 1\rangle$, $\langle 12\cdot 2\rangle$, and $\langle \bar{1}1\cdot 1\rangle$ axes, however, were in general kinked and nonuniform. For these whiskers the angles between the initial fcc axes and the observed hcp axes varied as much as 15 deg. This indicates that the atomic shift due to the alignment of the

[28] R. D. Dragsdorf and W. W. Webb, J. Appl. Phys. **29**, 817 (1958).
[29] J. D. Eshelby, Phil. Mag. **3**, 440 (1958).
[30] C. S. Barrett, *Structure of Metals* (McGraw-Hill Book Company, Inc., New York, 1952), p. 95.

TABLE I. Relationships between the axes[a] of the initial fcc whiskers and the observed hcp whiskers.

Initial fcc growth axis	Angle between normal to slip plane and growth axis (deg)	Related hcp axes		Number of whiskers observed	Angle between fcc axis and obs. hcp axis (deg)
		exact	approx		
110	90	10·0	10·0	48	0
	36	24·3	11·1	4	15
			12·2	1	7
100	55	$\bar{4}4\cdot3$	$\bar{1}1\cdot1$	4	6
111	0	00·1	00·1	3	0
	71	$\bar{8}8\cdot3$	$\bar{2}2\cdot1$	0	...

[a] The generalized set of axes in both the fcc and hcp system are specified.

observed crystallographic axes along the geometrical axes of these whiskers resulted in distorting the geometrical shape. Similar results have been reported by Gedwill *et al.*[31] for whiskers grown from $CoBr_2$.

Crystal Faces

The planes observed to form the crystal faces parallel to the whisker axes are listed in Table II. These planes are related in Table III to the {100}, {110}, and {111} planes in the fcc phase. The observed crystal faces and axes were compared to all possible combinations that could have resulted from the initial fcc whiskers. It was found that the transformation was influenced by the crystal boundaries. The formation of the ⟨10·0⟩, ⟨11·1⟩, and ⟨12·2⟩ hcp axes from whiskers with initial ⟨110⟩ fcc axes best illustrates the effect of the crystal boundaries. When either the combination of (001), $(\bar{1}11)$, and $(1\bar{1}1)$ planes or $(\bar{1}11)$ and $(1\bar{1}1)$ planes formed the crystal boundaries of the initial [110] whisker, the resulting hcp whisker had the [10·0] axis. For the initial combination of (001) and $(\bar{1}10)$ fcc surface planes the $[\bar{1}\bar{2}\cdot2]$, ⟨12·2⟩, hcp axis resulted. The $[0\bar{1}\cdot1]$, ⟨11·1⟩, whisker was obtained when the initial crystal faces were the combination of the (001) and $(1\bar{1}1)$ planes. The crystal boundaries then controlled the atomic movements resulting in the different observed axes. In all cases the transformation occurred on the set of {111} planes which resulted in the combination of surface planes of densest packing for the hcp crystal. This explains why the ⟨00·1⟩ axis rather than the $\langle\bar{2}2\cdot1\rangle$ axis was observed to result from the initial ⟨111⟩ fcc whisker. The surface planes of the resulting ⟨00·1⟩ whisker were of denser packing than those for the $\langle\bar{2}2\cdot1\rangle$ axis system.

TABLE II. Crystal faces and slip band orientations.

hcp whisker axis	Observed combinations forming crystal faces	Angle[a] between slip bands and whisker axis (deg)
10·0	$\begin{pmatrix}00\cdot2\\01\cdot\bar{1}^b\\01\cdot\bar{1}^b\end{pmatrix}$ and $\begin{pmatrix}00\cdot2\\01\cdot\bar{1}^b\end{pmatrix}$	... 0 0
11·1	$\begin{pmatrix}1\bar{1}\cdot0^b\\10\cdot\bar{1}\end{pmatrix}$ and $\begin{pmatrix}1\bar{1}\cdot0^b\\\\11\cdot\bar{2}^b\end{pmatrix}$	58 75 90
12·2	$\begin{pmatrix}01\cdot\bar{1}\\\bar{2}1\cdot0^b\end{pmatrix}$	90 62
$\bar{1}1\cdot1$	$\begin{pmatrix}10\cdot1\\0\bar{1}\cdot1\end{pmatrix}$	51 51
00·1	$\begin{pmatrix}11\cdot0^b\\\bar{1}2\cdot0^b\\\bar{2}1\cdot0^b\end{pmatrix}$	90 90 90

[a] Calculated values listed for interception of (00·1) plane with whisker face. Observed values were within 3° of those listed.
[b] Planes on which the most pronounced slip band formations were observed.

Slip Bands

The slip band formations on the surfaces of several whiskers are shown in Fig. 1. The slip bands on a particular surface are parallel, suggesting that the transformation occurred on only one set of {111} planes. The sequence of slip band formations on a

TABLE III. Correlation of the initial fcc axes and crystal faces to the transformation plane and resulting hcp axes.

Initial fcc whisker axis	Combination of fcc surface planes forming whisker boundaries	Transformation planes	Resulting hcp whisker axis[a]
110	001, $\bar{1}11$, $1\bar{1}1$	$\bar{1}11$ or $1\bar{1}1$	10·0
	$\bar{1}11$, $1\bar{1}1$	$\bar{1}11$ or $1\bar{1}1$	10·0
	001, $\bar{1}10$	111 or $11\bar{1}$	12·2
	001, $1\bar{1}1$	111 or $11\bar{1}$	11·1
100	010, 001	111, $\bar{1}11$, $1\bar{1}1$, or $11\bar{1}$	$\bar{1}1\cdot1$
111	$10\bar{1}$, $01\bar{1}$, $1\bar{1}0$	111	00·1
	$10\bar{1}$, $01\bar{1}$, $1\bar{1}0$	$\bar{1}11$, $1\bar{1}1$, or $11\bar{1}$	$\bar{2}2\cdot1^b$

[a] Generalized set of axes for the hcp system.
[b] Not observed.

[31] M. A. Gedwill, C. J. Altstetter, and C. M. Wayman, Trans. AIME **230**, 453 (1964).

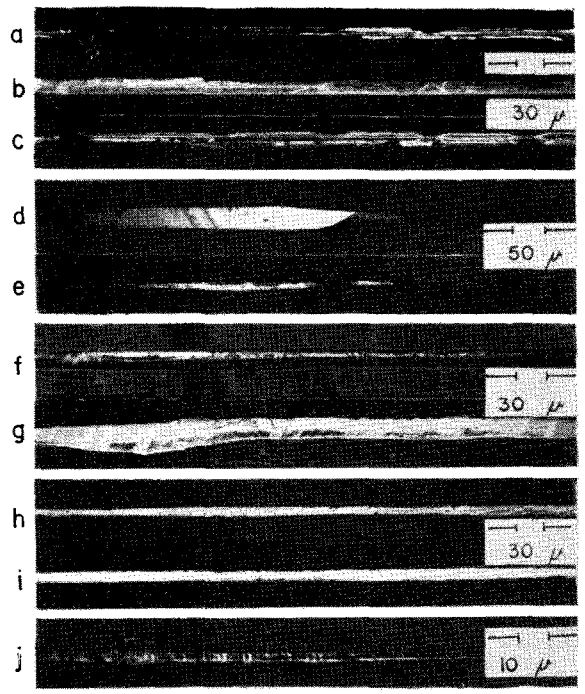

FIG. 1. Optical photographs of slip bands on surfaces of several cobalt whiskers. (a), (b), and (c): The (01·1), (00·2), and (0$\bar{1}$·$\bar{1}$) surface planes, respectively, of a [10·0] whisker, Co-117. The slip bands are parallel to the whisker axis. (d) and (e): The (1$\bar{1}$·0) and (11·$\bar{2}$) surface planes of a [11·1] whisker, Co-208, with slip bands at 58° and 90° to the whisker axis, respectively. (f) and (g): The (01·$\bar{1}$) and ($\bar{2}$1·0) surface planes of a [12·2] whisker, Co-50, with slip bands at 90° and 62° to the whisker axis, respectively. (h) and (i): The (10·1) and (0$\bar{1}$·1) surface planes of a [$\bar{1}$1·1] whisker, Co-58. There are no pronounced slip bands on these surfaces. (j): The (11·0) surface plane of a [00·1] whisker, Co-61. The slip bands are perpendicular to the whisker axis.

particular face did not identically correspond to that on the opposite face. This suggests either that some of the martensitic plates terminate within the crystal or that a slight amount of cross slip was present. The separation between slip bands varied from 2 to 10 μ, with 4 μ being most frequently observed. The planes upon which slip band formations were most frequently observed are noted in Fig. 1 and listed in Table II.

Axial Screw Dislocations

Cobalt whiskers contain an axial screw dislocation or dislocations in the initial fcc growth phase.[27] Diffraction from a whisker, Co-105, which retained most of the uniform lattice twist from an axial screw dislocation after the transformation to the hcp phase is shown in Fig. 2. A tilted equatorial Laue spot is shown in Fig. 2(a). Figures 2(b)–2(e) record high-resolution diffraction topographs from planes parallel to the whisker axis. The topograph in Fig. 2(b) has two distinct images resulting from diffraction of the $K\alpha_1$ and $K\alpha_2$ radiation. The Burgers vector for this axial screw dislocation was 5 Å which corresponds to two lattice translations along the [10·0] whisker axis. Diffraction from planes perpendicular to the axis of this whisker is recorded in Figs. 2(f)–2(h). The $K\alpha_1$ and $K\alpha_2$ diffraction is resolved in the topograph in Fig. 2(g). Figure 2(h) is an oscillation photograph. These topographs reveal strained regions at both the tip and base of this whisker.

Segmented Twist

The axial screw dislocation in the majority of cobalt whiskers was either partially or completely lost during

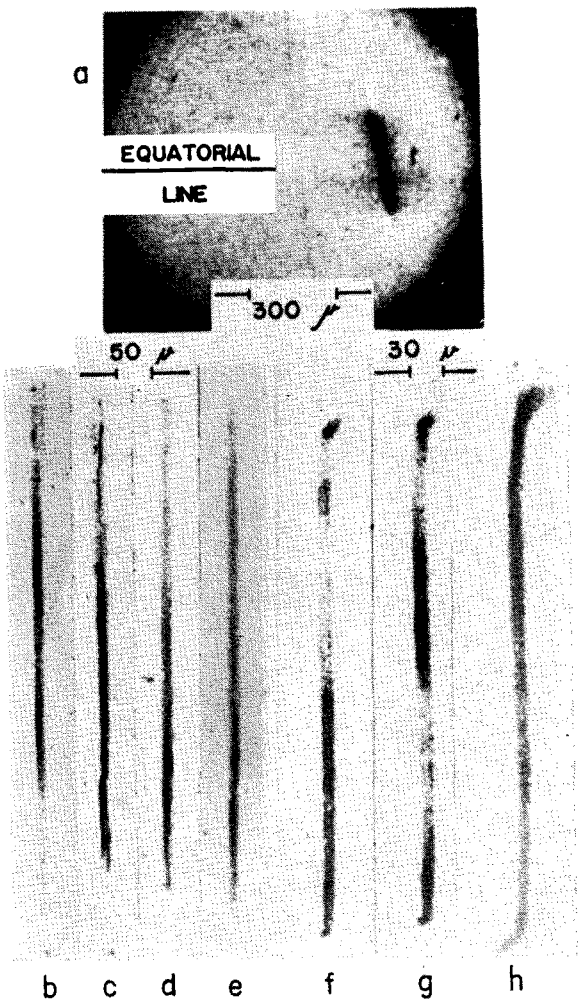

FIG. 2. X-ray diffraction profiles from a [10·0] whisker, Co-105. (a): Equatorial Laue spot showing the tilt resulting from an axial screw dislocation with a Burgers vector of 5 Å. (b) through (e): Topographs from the (00·2), (00·$\bar{2}$), (01·1), and (0$\bar{1}$·0) planes, respectively, parallel to the whisker axis which record variations in the diffracted intensity from strained regions in the crystal. Separation of the $K\alpha_1$ and $K\alpha_2$ diffraction profiles is observed in topograph (b). Variations in the diffracted intensity from other lattice distortions are most pronounced in the {00·2} topographs. (f), (g), and (h): Diffraction images from the ($\bar{2}$1·0) planes perpendicular to the whisker axis revealing strain at the tip and base of the whisker. (f) and (g) are topographs from different sections of the crystal, while (h) is an oscillation photograph.

the transformation from the initial fcc growth phase to the resulting hcp phase. The partial relief of the strain associated with the lattice twist was revealed by the segmented structure of the equatorial Laue spots. Diffraction from one of many segmented whiskers is shown in Fig. 3. This whisker had a [10·0] axis and gave no external indication of fragmentation other than slip band formations on the surfaces. The degree of segmentation perpendicular to the whisker axis is, however, quite severe. The equatorial Laue spot of Fig. 3(a) shows a block-like structure. The blocks are rotated relative to one another in such a manner that a tilted diffraction image occurs. Topographs, Figs. 3(b)–3(i), and the oscillation photograph, Fig. 3(j), of this whisker give an indication of the complexity of the strained lattice structure. Orientations differing by as much as 18 min of arc about the (00·2) diffraction peak are seen in the topographs of Figs. 3(b)–3(e).

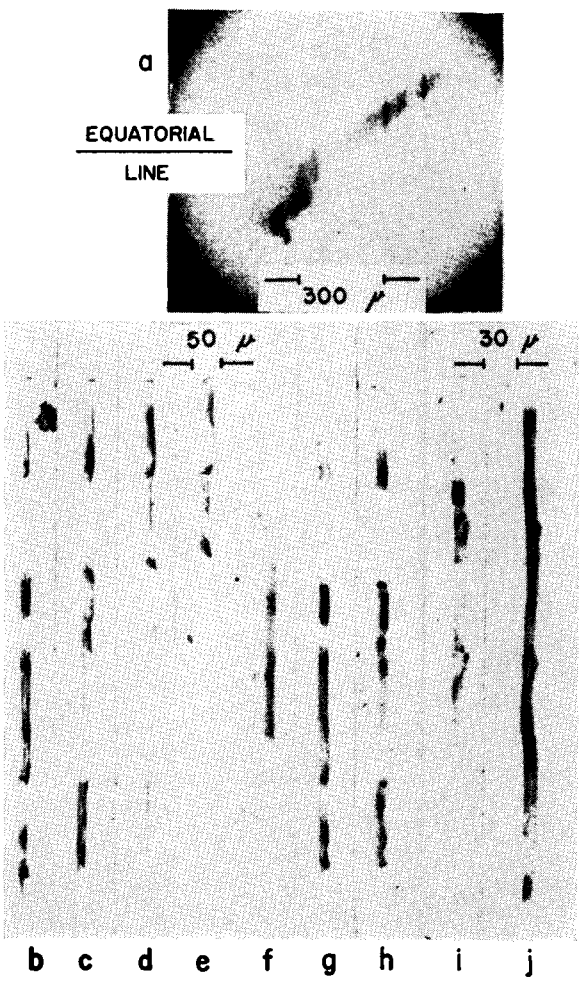

FIG. 3. X-ray diffraction profiles from a [10·0] whisker, Co-117. (a): Equatorial Laue spot showing a segmented tilt. (b) through (h): diffraction topographs showing severe segmentation perpendicular to the whisker axis. The diffraction is from planes parallel to the whisker axis. Topographs (b), (c), (d), and (e) are from the (00·2) planes with relative angular orientations of 0, 6, 12, and 18 min of arc, respectively. Topographs (f), (g), and (h) are from the (01·0), (01·$\bar{1}$), and (0$\bar{1}$·2) planes, respectively; (i) and (j) reveal the complexity of strain in several sections of the whisker. (i) is a topograph and (j) is an oscillation photograph from the ($\bar{2}$1·0) planes perpendicular to the whisker axis.

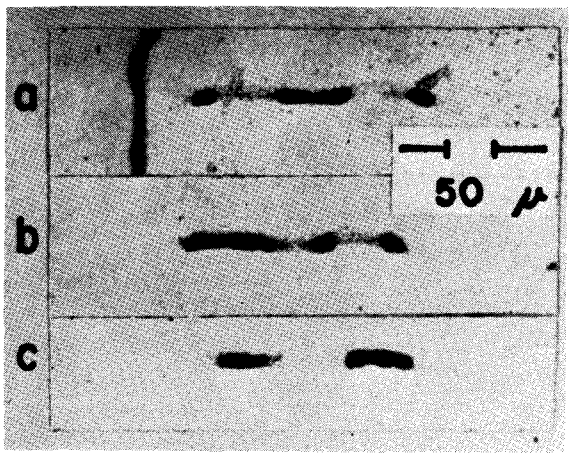

FIG. 4. X-ray diffraction topographs from the (00·2) planes of whisker, Co-105, at relative orientations of 0, 3, and 6 min of arc, respectively, showing the polycrystalline structure which resulted from recycling through the transformation. The heat treatment was at 450°C for 3 h in an H_2 atmosphere. Refer to topographs in Figs. 2(b) and 2(c) for history prior to heat treatment.

Temperature Cycling

Successive cycling of the hcp single-crystal whiskers through the transformation resulted in complete loss of the axial screw dislocations and the formation of oriented polycrystalline cobalt filaments. Diffraction topographs of whisker Co-105 after recycling to a temperature of 450°C for 3 h in an H_2 atmosphere are given in Fig. 4. The diffraction topographs of this whisker prior to the heat treatment were shown in Fig. 2.

Partial Dislocations

Partial dislocations have been identified from an analysis of the intensity contrasts in the diffraction profiles from cobalt whiskers. The diffraction from whiskers with a [10·0] axis was most readily interpreted. Topographs from [10·0] whiskers such as Co-105, Figs. 2(b)–2(e), and Co-117, Figs. 3(b)–3(h), show that the maximum intensity contrasts and detail are recorded in the diffraction profiles from the (00·2) planes. This suggests that the maximum lattice distortions are in directions normal to these planes. The product $\mathbf{b}\cdot\mathbf{G}$ is a maximum when $\mathbf{b}$ is normal to the (00·2) plane. For these lattice distortions diffraction from the (01·0) plane should show little or no contrast; since $\mathbf{b}\cdot\mathbf{G}=0$ for this case. Likewise, the recorded diffracted intensity contrasts from the (01·$\bar{1}$) and (0$\bar{1}$·2) planes should be intermediate be-

TABLE IV. Intensity contrast analysis for partial dislocations with residual Burgers vectors normal to the (00·1) plane.

Whisker axis	Whisker	Diffracting plane ($hk\cdot l$)	Observed contrast[a]	$\mathbf{b}\cdot\mathbf{G}/\lvert b \rvert\lvert G \rvert$ for **b** normal to the (00·1) plane
10·0	Co-117	01·0	W	0
		00·2	S	1.0
		01·$\bar{1}$	M	0.5
		0$\bar{1}$·2	M	0.7
12·2	Co-50	0$\bar{1}$·1	S	0.5
		$\bar{2}$1·0	W	0
11·1	Co-43	10·$\bar{1}$	S	0.5
		0$\bar{1}$·1	S	0.5
		1$\bar{1}$·0	W	0
$\bar{1}$1·1	Co-58	10·1	S	0.5
		0$\bar{1}$·1	S	0.5
		11·0	W	0

[a] Strong (S), medium (M), and weak (W).

tween the extreme contrasts observed from the (00·2) and (01·0) diffracting planes. These relative intensity contrasts are observed in the diffraction topographs from [10·0] cobalt whiskers. The results of the analysis of Co-117 are summarized in Table IV as an example of diffraction from a [10·0] whisker. Optical studies of [10·0] whiskers show that the most pronounced slip band formations do not occur on the (00·2) crystal face. Therefore, the plane which produces the maximum intensity contrast does not possess the most pronounced slip band formations.

Diffraction topographs from a [12·2] whisker, Co-50, show contrasting intensity variations in Fig. 5(a)–5(e). Contrasts within the (0$\bar{1}$·1) diffraction images [Figs. 5(a)–5(d)] are very pronounced and extended completely across the diffraction profiles. This is contrasted by the more uniform intensity distribution in the ($\bar{2}$1·0) diffraction profile seen in Fig. 5(e). Again, the recorded diffraction profiles show that the major lattice distortions are in directions normal to the (00·1) plane, see Table IV. Optical studies of this whisker [Figs. 1(f) and 1(g)] show that the most pronounced slip band formations are seen on the ($\bar{2}$1·0) crystal face.

Topographs from a [11·1] whisker, Co-43, and from a [$\bar{1}$1·1] whisker, Co-58, are given in Figs. 5(f) through 5(p). A summary of the findings is also included in Table IV. The results of the x-ray and optical studies were consistent with the observations on the other whiskers. For whisker Co-58 no slip bands are observed optically in Figs. 1(h) and 1(i) while faulted regions are clearly indicated in the x-ray topographs of Figs. 5(m)–5(p).

The x-ray and optical analysis of all cobalt whiskers showed that the maximum lattice distortions are in directions normal to the (00·1) planes. Some of the distortions are characterized by sharp contrast lines with widths as small as 3 μ within the x-ray topographs seen in Fig. 5. These line distortions result from Frank partial dislocations which are pinned in the hcp lattice and form the boundary of a faulted region in the crystal. The Frank partials have Burgers vectors normal to the (00·1) plane. In other regions of imperfection the x-ray intensity contrast is much reduced. Little contrast is seen within the diffraction maxima of the [10·0] whiskers as shown in Figs. 2 and 3. This is perhaps attributable to a mismatch of two parallel and adjacent sections of the crystal which had different sets of slip vectors on transformation and no pinned dislocations.

It is informative to examine the way in which the

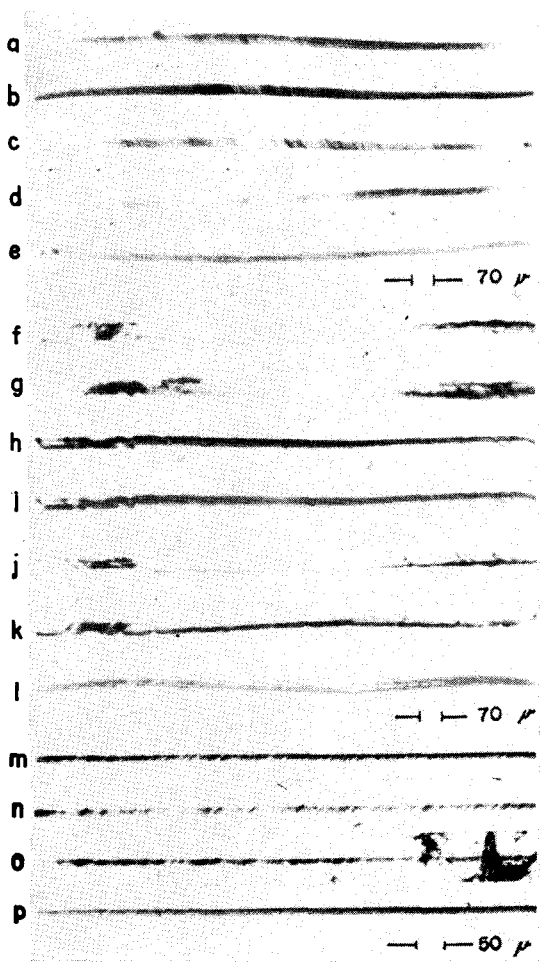

FIG. 5. Diffraction topographs showing variations in intensity from regions containing partial dislocations in several cobalt whiskers. The diffraction is from planes parallel to the whisker axis. The whiskers, diffracting planes, and relative angular orientations are: Co-50, [12·2] axis, (0$\bar{1}$·1) planes at (a) 293°0′ (b) 293°6′, (c) 293°12′, and (d) 113°0′, (e) ($\bar{2}$1·0) planes at 5°15′; Co-43, [11·1] axis, (10·$\bar{1}$) planes at (f) 60°3′ and (g) 240°3′, (0$\bar{1}$·1) planes at (h) 292°24′, (i) 292°27′, (j) 292°30′, and (k) 112°30′, (l) (1$\bar{1}$·0) planes at 359°42′; Co-58, [$\bar{1}$1·1] axis, (10·1) planes at (m) 0°0′ and (n), 0°6′ (o) (0$\bar{1}$·1) planes, (p) (11·0) planes.

Frank partial dislocations were formed. The initial [110] and [100] fcc cobalt whiskers contained axial screw dislocations with $\frac{1}{2}[110]$ and [100] Burgers vectors, respectively. During the transformation, these total dislocations become resolved into a set of partial dislocations. Table V records: (1) sets of possible partial dislocation combinations that can result from these axial screw dislocations; (2) the resulting hcp whisker axes for the transformation occurring on the appropriate {111} plane; and (3) ratio of the sum of the energy of the two partials to the energy of the total dislocation. The energy is approximated to be proportional to the square of the Burgers vector.[26] This method of energy determination predicts a reduction in energy accompanying the formation of partials for only two of the cases considered. The most energetically favorable combinations occur when the axial screw dislocation becomes extended into two Shockley partial dislocations. The slip associated with these partials would result in a ⟨10·0⟩ whisker axis as shown in Table V. This is verified experimentally in that 80% of the whiskers examined had such axes. The energy determinations show no energy decrease for the cases where both Shockley and Frank partials are formed. These combinations can still be realized, however, since the energy needed to extend the total dislocations could come from the free-energy difference between the two phases during the transformation.

These results suggest that even though the Frank partial dislocations are pinned in the lattice, the Shockley partial dislocations move by glide through the lattice and are lost at the surface. The Burgers vectors of the Shockley partials are parallel to the transformation slip vectors. The precise slip vectors were identified for fourteen whiskers by relating the experimentally determined axial screw dislocations and the Frank partial dislocations through the equalities in Table V.

TABLE V. Formation of partial dislocations from the extension of the axial screw dislocation in cobalt whiskers.

Slip plane	Dislocation reaction relating Burgers vectors[a] (axial screw to two partials)	Resulting hcp whisker axes	Energy[b] ratio (partials to axial screw)
111	$\frac{1}{2}[110]=\frac{1}{6}[111]+\frac{1}{6}[11\bar{2}]$	$\bar{1}\bar{2}\cdot 2:\bar{1}\bar{1}\cdot 1$	1
$\bar{1}11$	$\frac{1}{2}[110]=\frac{1}{6}[12\bar{1}]+\frac{1}{6}[211]$	$\bar{1}0\cdot 0$	$\frac{2}{3}$
$1\bar{1}1$	$\frac{1}{2}[110]=\frac{1}{6}[121]+\frac{1}{6}[21\bar{1}]$	$10\cdot 0$	$\frac{2}{3}$
$11\bar{1}$	$\frac{1}{2}[110]=\frac{1}{6}[11\bar{1}]+\frac{1}{6}[112]$	$\bar{2}\bar{1}\cdot 2:\bar{1}\bar{1}\cdot 1$	1
111	$[100]=\frac{1}{3}[111]+\frac{1}{3}[2\bar{1}\bar{1}]$	$\bar{2}\bar{1}\cdot 1$	1
$\bar{1}11$	$[100]=\frac{1}{3}[1\bar{1}\bar{1}]+\frac{1}{3}[211]$	$\bar{1}1\cdot\bar{1}$	1
$1\bar{1}1$	$[100]=\frac{1}{3}[1\bar{1}1]+\frac{1}{3}[21\bar{1}]$	$1\bar{1}\cdot 1$	1
$11\bar{1}$	$[100]=\frac{1}{3}[11\bar{1}]+\frac{1}{3}[2\bar{1}1]$	$\bar{1}\bar{2}\cdot 1$	1

[a] ⟨211⟩ are slip directions and are parallel to the Burgers vectors of Shockley partial dislocations. ⟨111⟩ directions are parallel to the Burgers vectors of the Frank partial dislocations.

[b] The energy is approximated to be proportional to the square of the Burgers vector.[26]

DISCUSSION AND CONCLUSIONS

The observed hcp whiskers were single crystals and had parallel slip band formations on the crystal faces. The atomic movements during the transformation were confined to only one of the four possible sets of {111} close-packed planes. Analysis of the whisker axes and crystal boundaries yielded the general result that the fcc to hcp transformation occurred on the particular set of {111} planes which gave the combination of surface planes of densest packing for the resulting hcp whiskers. Thus the surface planes of the initial fcc crystal and the resulting surface planes of densest packing in the hcp whisker played an important role in defining the slip plane. Dehlinger *et al.*[15] have suggested that the transformation to the hcp phase occurs preferentially on the {111} planes with the greatest surface area. This does not satisfactorily explain the transformation as observed in cobalt whiskers, e.g., the transformation resulting in the ⟨11·1⟩ whisker did not occur on the close-packed plane forming a face of the initial fcc whisker. These results are further supported by the work of Nelson and Altstetter[32] which showed that for large single crystals of cobalt the {111} plane of maximum surface area is not necessarily the transformation plane. The transformation in cobalt whiskers is not defined by one close-packed surface plane, but by the combination of all planes forming the faces of the crystal.

The stress resulting from an axial screw dislocation could act to restrict the atomic movements during the transformation to the {111} planes most nearly parallel to the whisker axis. Such slip would decrease the lattice strain caused by the dislocation, so that little or no lattice twist would remain after the transformation was complete. The transformation planes giving rise to only the ⟨10·0⟩ and ⟨$\bar{1}$1·1⟩ axes are in complete agreement with this slip direction. The role of the axial screw dislocation as a transformation restricting mechanism was better defined from the heat treatment studies. Successive cycling of the hcp single-crystal whiskers through the transformation resulted in complete loss of the axial screw dislocation and the formation of oriented polycrystalline cobalt filaments. These polycrystalline or fragmented specimens were formed as a result of the transformation on more than one set of {111} planes. In cobalt whiskers the loss of the axial screw dislocation was definitely associated with the loss of a transformation restricting mechanism.

High-resolution x-ray diffraction topographs revealed that the most pronounced lattice distortions in cobalt whiskers were in the [00·1] direction which

[32] J. O. Nelson and C. J. Altstetter, Trans. AIME **230**, 1577 (1964).

is normal to the plane containing the martensitic platelets. These distortions were formed during the transformation and resulted from the resolution of the initial axial screw dislocation into two partial dislocations. At least one of these dislocations was a Shockley partial which glided through the lattice and completed the fcc to hcp transformation. This implies that the transformation initiated at the site of the axial screw dislocation. For $\langle 12\cdot 2\rangle$, $\langle 11\cdot 1\rangle$, and $\langle \bar{1}1\cdot 1\rangle$ whiskers the second partial dislocation was a Frank partial with a Burgers vector perpendicular to the slip plane. This partial dislocation could move only by climb and as a result remained pinned in the lattice. The Frank partial dislocations form the boundary of the faulted regions which terminate within the crystal. These faulted regions make up the martensitic platelets. For the $\langle 10\cdot 0\rangle$ whiskers, however, both partial dislocations are Shockley partials and the platelets were formed as a result of the mismatch of two parallel sections which had different transformation slip vectors.

SUMMARY

Cobalt whiskers reported in this study were grown in the high-temperature fcc phase but were cooled through the phase transformation to the hcp structure before being examined at room temperature. These whiskers grew by a screw dislocation mechanism and had $\langle 110\rangle$, $\langle 100\rangle$, and $\langle 111\rangle$ growth axes and combinations of $\{110\}$, $\{100\}$, and $\{111\}$ planes as crystal faces. The transformation from the as-grown fcc whisker to the hcp whisker initiated at the site of the axial screw dislocation. The strain associated with the axial screw dislocation and the boundary conditions imposed by the crystal faces act as a combined mechanism restricting the transformation to only one of the four sets of $\{111\}$ fcc planes. The transformation occurred on the particular set of planes which gave surface planes of densest packing in the resulting hcp whisker. The atomic movements during the transformation resulted in the partial or complete loss of the axial screw dislocation and in the formation of slip bands. The axial screw dislocation was resolved into two partial dislocations, at least one of which was a Shockley partial. This partial glided through the lattice and completed the fcc to hcp transformation. Loss of the axial screw dislocations reduced the strain in the system. The strain that did remain, however, was associated either with Frank partial dislocations which remained pinned in the lattice or with a mismatch between subdomains which resulted from two different slip directions on the same close-packed planes. Upon recycling through the transformation, without the axial screw dislocation restricting mechanism, each localized region of strain and the crystal boundaries defined a set of transformation planes. Atomic slip occurred then on more than one set of $\{111\}$ planes resulting in polycrystalline filaments.